Improving NSCAT Winds for Tropical Cyclones

Simon H. Yueh, Wu-Yang Tsai, Carol S. Hsu, Hua Hu and W. Timothy Liu
Jet Propulsion Laboratory, California Institute of Technology, Pasadena, California

Short title: IMPROVING NSCAT WINDS FOR TROPICAL CYCLONES

Abstract.

There has been a question on whether it is possible to measure the surface wind speeds of tropical cyclones with a spaceborne Ku-band scatterometer. This paper explores the accuracy of NSCAT winds for tropical cyclones (TCs) through a comparative analysis of NSCAT winds, the best track records obtained from Joint Typhoon Warning Center (JTWC) and National Hurricane Center (NHC), SSM/I rain rates and Holland's TC model. The high wind portion of the NSCAT2 geophysical model function (GMF) is adjusted based on a set of aircraft scatterometer observations. The NSCAT measurements of 12 Western Pacific and 2 Atlantic cyclones were processed with the modified geophysical model function (NSCAT/TC2). It is found that the NSCAT wind speeds can reach as high as 40-50 $m \cdot s^{-1}$ for many cases, in better agreement with what is expected for typhoons and hurricanes. The resulting NSCAT winds as compared with the SSM/I rain rates suggest a significant impact of rain, which appears to make the scatterometer winds lower than expected for tropical cyclones. The comparison is supported by a radiative transfer modeling of rain and Holland's TC model field. The analysis also suggests that the NSCAT winds are reasonable for the areas with low rain rates. The comparison of the NSCAT maximum wind speeds and Holland's TC model winds shows that it is possible to estimate hurricane winds with a spaceborne Ku-band scatterometer. However, ancillary data for rain flagging are clearly necessary.

1. Introduction

Skillful forecasts of the tropical cyclone (TC) track and intensity depend on a proper depiction of the initial air and sea states in TC forecast models [*Bender et al.* 1993]. A primary source of difficulty in past efforts for TC forecasting has been the inability to make direct observations of the surface wind field, which is one of the key driving forces for the heat and moisture exchange between the air and sea surfaces [*Hsu and Liu,* 1996, *Dickinson and Brown,* 1996, *Hsu et al.,* 1997]. Currently, the major data source for TC forecasting is the geostationary satellite visible and infrared images. The technique developed by [*Dvorak,* 1975] (hereafter referred to as the Dvorak technique), analyzing the cloud features in the visible and IR imageries, yields the estimates of maximum wind speed and central pressure, but does not provide the spatial distribution of surface winds, which is necessary for the analysis of surface wind divergence and vorticity.

Two other data sources for TC forecasting are from satellite microwave radiometers and scatterometers. Satellite microwave radiometers, including the Multichannel Microwave Radiometer (SMMR) flown on NIMBUS-7 and SEASAT and the Special Sensor Microwave/Imager (SSM/I) deployed on the Defense Meteorological Satellite Program (DMSP) missions, have been providing global ocean surface wind speeds since 1978. However, the extreme sensitivity of microwave brightness temperatures to precipitation makes it difficult to use passive microwave radiometer observations for the estimates of tropical cyclone surface wind speeds.

Satellite scatterometers are less sensitive to rain and clouds than microwave radiometers. The capability of satellite scatterometers was demonstrated in 1978 by the Seasat Scatterometer (SASS), which operated at Ku-band (14.6 GHz). Since 1991, two European Earth Remote Sensing Satellite (ERS-1 and -2) scatterometers have been launched by the European Space Agency (ESA). Several ERS-1 scatterometer passes of the Western Pacific TCs [*Quilfen et al.* 1998] suggest that the ERS-1 computed

maximum wind speeds are lower than those derived from the Dvorak technique by about 20-40 $m \cdot s^{-1}$. It was postulated by [*Quilfen et al.* 1998] that three major error sources are limiting the high wind measurement performance of ERS scatterometers:

1. Deficiencies of the geophysical model function (GMF) for high winds,
2. Effects of heavy rain on the microwave attenuation and the roughness of sea surfaces, and
3. Wind gradient in the sensor footprint near the eyewall where the maximum wind speeds are expected.

Here, we study the high wind measurement performance of the NASA Scatterometer (NSCAT) on-board the Japanese Advanced Earth Remote Sensing Satellite (ADEOS-1) from September 1996 through June 1997. NSCAT operated at Ku-band (13.995 GHz), which is more sensitive to ocean winds, but is expected to be more susceptible to rain than the C-band frequencies employed by ERS scatterometers. Because of the superior resolution of NSCAT (25 km) compared with the ERS scatterometer footprint size of 50 km, the effects of wind gradient are less critical for NSCAT. Therefore, we focus on the deficiencies of the scatterometer GMF and explore the influence of precipitation on NSCAT observations.

Our approach is to improve the high wind portion of NSCAT GMF with a set of aircraft scatterometer measurements. Subsequently, we process the NSCAT backscatter measurements with the improved Ku-band GMF for 12 Western Pacific and 2 Atlantic cyclones. Finally, the accuracy of NSCAT TC winds is evaluated with a comparative analysis of the Dvorak wind speeds obtained from the Joint Typhoon Warning Center (JTWC) and National Hurricane Center (NHC), the SSM/I rain rates, and Holland's TC model fields [*Holland*, 1980; *Young*, 1993].

In the next section, we describe the improved Ku-band GMF for NSCAT data processing. Section 3 describes the comparative analysis of NSCAT, SSM/I, JTWC and

NHC Dvorak winds, and Holland's TC model fields. An error analysis is described in Section 4. Discussions and summary are given in Section 5.

2. Ku-Band Geophysical Model Function

A scatterometer is a microwave radar designed to measure the ocean surface wind velocity. It transmits a short microwave pulse and receives the echo from ocean surfaces. This radar echo has been found to be sensitive to the ocean surface waves generated by the surface wind. To facilitate the retrieval of surface wind velocities from radar measurements, an empirical geophysical model function (GMF) relating the normalized radar cross-section (σ_0) to the surface wind velocity is employed by the NSCAT data processing system.

The primary approach for the derivation of a satellite scatterometer GMF relies on the combined analysis of satellite scatterometer measurements, numerical model wind fields and buoy winds. The NSCAT2 GMF developed by [*Wentz et al.* 1998] uses the full set of NSCAT backscatter data and the model fields from the National Centers for Environmental Prediction, while the C-band ERS GMFs, CMOD4 [Stoffelen and Anderson, 1997] and CMOD_IFR2 [*Quilfen et al.* 1998], are based on an analysis of the European Centre for Medium-Range Weather Forecasts (ECMWF) analysis and buoy winds. There is a good agreement between the buoy and scatterometer winds at less than 20 $m \cdot s^{-1}$ [*Wentz et al.* 1998; *Rufenach,* 1997]. However, as indicated in [*Quilfen et al.,* 1998], the lower than expected CMOD4 and CMOD_IFR2 winds for tropical cyclones suggest a large uncertainty of scatterometer GMFs derived from numerical model fields and buoys for high winds.

The inaccuracy of the NSCAT2 GMF for high winds is suggested by the ocean backscatter measurements acquired by the Jet Propulsion Laboratory (JPL) Ku-band dual-polarized scatteroemter (NUSCAT) deployed during the Hurricane Ocean Wind Experiment (HOWE) 1997, which was designed to explore the polarization signatures

of Ku-band ocean backscatter and polarimetric microwave radiometer signals for high winds. This experiment was organized by the Jet Propulsion Laboratory (JPL) in conjunction with the Naval Research Laboratory (NRL) with a set of aircraft flights over Hurricane Erika in September 1997. The HOWE sensor suite includes the JPL Ku-band dual-polarized scatterometer (NUSCAT), JPL polarimetric 17, 19 and 37 GHz radiometers, NRL X-band polarimetric radiometer, the University of Massachusetts (UMASS) C- and Ku-band scatterometers (C-Scat and Ku-Scat), and the contributions from several other institutions. The surface truth was obtained by a direct measurement of wind velocity (speed and direction) along with several other meteorological parameters with the GPS dropsondes. Details of the NUSCAT/HOWE data set are described in [*Yueh et al.,* 1998]. The data from the (19 and 37 GHz) radiometer deployed together with the NUSCAT have been used to provide a correction of atmospheric attenuation on the NUSCAT backscatter measurements. It was found that the horizontal polarization has a greater sensitivity to wind speed and direction than the vertical polarization for high winds, but apparently also has a larger modeling uncertainty. Fig. 1 depicts a set of coincidental NUSCAT and radiometer data acquired at a wind speed of about 35 $m \cdot s^{-1}$. The location of this flight had broken scattered clouds, consistent with what is suggested by the radiometer data. There were clear wind direction signals in the NUSCAT σ_{vv} (vertically polarized transmit and vertically polarized receive), σ_{hh} (horizontally polarized transmit and horizontally polarized receive), and σ_{hv} (vertically polarized transmit and horizontally polarized receive). It is shown that σ_{hh} has a stronger azimuthal modulation than σ_{vv} by about 50 percent with an upwind and crosswind asymmetry of about 3 dB for σ_{hh} and about 2 dB for σ_{vv}. The cross-polarized backscatter σ_{hv} also has a wind directional dependence, but appears to be more susceptible to other scattering phenomena. Another set of data (Fig. 2) was acquired at an area with about 5-10 mm/h rain rate. The 37 GHz radiometer data were near saturation and the NUSCAT backscatter data were probably influenced by rain

with no consistent directional variations. The aircraft NUSCAT flight data do support the possibility of dual-polarized Ku-band radar for hurricane ocean wind measurements, but the data also suggest a reduced wind speed and direction sensitivity in the high wind regime and the impact of rain.

Figs. 3 and 4 illustrate the NUSCAT σ_0 acquired at above 20 m·s^{-1} and the predictions by the NSCAT2 GMF. It appears that the NSCAT2 GMF predicts higher σ_0s and stronger directional σ_0 variations for hurricane winds. This is consistent with the indications that the NSCAT2 winds remain lower than expected for tropical cyclones.

To make a first-order correction, we introduced a product model to lower the high wind portion of the NSCAT2 GMF. The upwind σ_0 from the NSCAT2 GMF is multiplied by a function f, which reduces to one for low and moderate winds and decreases with increasing wind speeds. Namely, the modified upwind model σ_0' is related to the NSCAT2 upwind σ_0 by

$$\sigma'_{0up} = f(\theta, W, p)\sigma_{0up} \tag{1}$$

where θ is the incidence angle, W is the wind speed, and p indicates the polarization. The empirical correction term takes the following form

$$f(\theta, W, p) = 1 - \exp[-(W_c/W)^{\beta/2}] \tag{2}$$

where

$$W_c = 55 + 4000\exp[-(\theta - 15)^2/20] \tag{3}$$

$$\beta = -2.575 + 0.2621\theta - 4.8020 \times 10^{-3}\theta^2 + 2.936027 \times 10^{-5}\theta^3 \tag{4}$$

The functional form and coefficients of W_c and β, were selected using the NUSCAT data and through a qualitative examination of the NSCAT winds for Hurricane Lili. Based on the suggestions of NUSCAT data, we tune the model coefficients to reduce the modeling σ_0. We process the NSCAT data from the Hurricane Lili and adjust the

coefficients until the NSCAT maximum wind speed appears consistent with the NHC best track analysis and ship observations of Hurricane Lili. It will be shown in the following analysis that the proposed corrections make the NSCAT winds for the Western Pacific tropical cyclones in better agreement with the JTWC best track analysis.

In addition to the tuning of NSCAT2 σ_{0up}, we find that the ratio of NSCAT2 upwind and crosswind σ_0s for high winds requires adjustments. It is indicated in Fig. 4 that the ratio of NSCAT2 upwind and crosswind σ_0s was set to a constant for wind speeds above 23 m·s^{-1}, apparently due to a lack of higher wind speeds in the NCEP analysis. This is inconsistent with the expected directional distribution of short ocean waves described in [*Liu and Yan,* 1995], which suggested that several dissipation processes can result in saturated amplitudes and more isotropic orientation of short waves for high winds (> 20 m·s^{-1}). This implies that the upwind and crosswind σ_0 ratio should decrease with increasing wind speed for high winds. Hence, we model the upwind and crosswind σ_0 ratio (r_{uc}) in decibel (dB) with the following functional form:

$$r_{uc}(dB) = c\{1 - \gamma_1 \exp[-(W/a)^{\alpha}]\}\{1 - \gamma_2 \exp[-(b/W)^{\beta}]\} \tag{5}$$

The term in the first pair of braces, increasing with wind speed, accounts for the rising r_{uc} from low to about 15 m·s^{-1}, while the term in the second pair of braces models a reducing r_{uc} with wind speed. The modeling coefficients, c, a, b, α, β, γ_1, and γ_2 are parameterized by a third-order polynomial function of the incidence angle θ. Tables 1 and 2 illustrate the polynomial coefficients for both polarizations. It is indicated in Fig. 4 that this model provides a good agreement with the vertically polarized NUSCAT data acquired at above 23 m·s^{-1} wind speeds. A comparison for horizontal polarization has been performed, and the results are similar.

Fig. 4 also illustrates the ratio of upwind and downwind σ_0s (r_{ud}). We find that the NSCAT2 r_{ud}, which is small for high winds and may become negative at small incidence angles, are fairly consistent with the NUSCAT measurements. The difference is small

and hence, no adjustment is applied.

The modified GMF is assumed to take the same form with the NSCAT2 GMF, which is modeled by a truncated cosine series of the wind direction (ϕ):

$$\sigma_0 = \sum_{n=0}^{5} A_n \cos n\phi \tag{6}$$

From the NSCAT2 GMF and the empirical corrections described above, we evaluate σ'_{0up}, r_{uc}, and r_{ud} for each incidence angle, wind speed and polarization and make the ratios A_3/A_0, A_4/A_0 and A_5/A_0 to be the same as those of the NSCAT2 GMF. This allows us to calculate the coefficients of the truncated cosine series for the modified NSCAT GMF, referred to as the NSCAT/TC2 GMF in this article.

3. NSCAT TC Winds

NSCAT operated six antenna fan beams to illuminate a swath width of 600 km on each side of the spacecraft nadir track [*Naderi et al.*, 1992]. The fore- and aft-beam antennas operate at vertical polarization, while the mid-beam antennas acquire vertically and horizontally polarized backscatter. The return echo from each antenna was Doppler-filtered to produce 25 σ_0s. One of the σ_0s is located near the spacecraft track with a nominal incidence angle of 10 ° for the monitoring of instrument stability and the other 24 σs are equally spaced between 200 km and 800 km off the nadir track. The resolution of each σ_0 footprint is 25 km (cross-track) by 7 km (along-track), superior to the ERS scatterometer resolution (50 km by 50 km), and hence the impact of wind gradient is expected to be smaller on NSCAT winds.

The σ_0 measurements from the fore-, mid- and aft-beam antennas are grouped into 25 km by 25 km bins for wind retrieval processing. We have processed the grouped NSCAT σ_0 data with the NSCAT/TC2 GMF for the typhoons and hurricanes indicated in Table 3. For those cyclones, the best track analysis was obtained from the JTWC and NHC for error analysis. The best track analysis includes the location (latitude and

longitude) and the Dvorak estimates of maximum wind speed for every six hours at 0, 6, 12, and 18 UTC. The number of NSCAT passes for each cyclone is indicated in the third column of Table 3. However, we found that the center of the cyclones frequently fell outside of the NSCAT swath and sometimes over land. For example, the typhoon Dale was a super typhoon with the maximum wind speed reaching 140 knots on November 9, 1996. There are a total of 12 NSCAT passes containing portion of the typhoon Dale from 6-12 November 1996, but only four of them had the center of the typhoon in the swath.

Fig. 5 illustrates the NSCAT wind images of typhoon Dale from these four satellite passes. The NSCAT resolution of 25 km appears to provide fairly details of the cyclone surface winds, indicating organized spiral patterns around the center of the cyclones (black filled circles). The NSCAT winds are in the expected counter-clockwise directions around the center of the cyclones in the northern hemisphere, except for a few areas where rain might have obscured the wind directional dependence of σ_0. The regions of maximum winds were located on the right hand side of the typhoon forward motion, consistent with what is generally expected for tropical cyclones.

Many regions in Fig. 5 indicate wind speeds in the range of 33 to 50 $m \cdot s^{-1}$, but around the high wind areas there could be lower than expected wind speeds. This is evident in the upper left panel of Fig. 5 of the NSCAT winds for typhoon Dale: The wind speeds in an area to the south of the eye appeared as low as 5 $m \cdot s^{-1}$. It is unlikely that the cyclone winds could be so low and asymmetric around the center, considering the strength of typhoon Dale. We suggest that the low wind areas appeared in the NSCAT/TC2 winds are influenced by the rain bands around the cyclone. Fig. 6 plots the daily averaged SSM/I wind speed, cloud liquid water path, water vapor and rain rate on November 7, 1996 together with the NSCAT winds and Holland's TC model fields. Because of the influence of rain on microwave brightness temperatures, no wind speeds were retrieved for a large area from the SSM/I brightness temperature data.

It appeared that rain also impairs the water vapor retrieval but for a smaller area. There is a rain band (red-orange colors) drawn into the center of the cyclone from the south west with heavy rain rates in the range of 10-25 mm/h. There was another rain band (green-blue colors) with 10-20 mm/h rain rate to the east of the eye, extending approximately in the north-south direction and spiraling toward the north west. These two heavy rain bands are strongly correlated with the spatial patterns of the NSCAT winds.

The Holland's TC model field [*Holland*, 1980; *Young,* 1993] is illustrated in Fig. 6 as a reference. Holland's TC model has been considered as a useful parametric model of the hurricane winds, and recently has been used by [*Young,* 1993] for the analysis of high wind altimeter measurements. Because this model has not considered the environmental flow (background field), the winds predicted from this model are not reliable for areas located too far from the eye. Therefore, we simulate the model fields at the locations of NSCAT bins within 200 km from the eye. Holland's TC model field is specified by six parameters: the latitude and longitude of the center, velocity of forward motion (speed and direction) V_{fm}, central pressure, and radius of the maximum winds. The JTWC best track records provide the latitude and longitude of the centers and the maximum wind speeds at 0, 6, 12, and 18 UTC. We linearly interpolate from the best track analysis to find the location of the center and V_{fm} at the time of NSCAT pass. We find that the maximum wind speed of the Holland's TC model is dominated by the central pressure for slowly moving systems. The radius of the maximum wind is adjusted so that the size of TC model field indicated by orange-yellow colors agrees with the NSCAT field.

The NSCAT wind directions have a good agreement with Holland's model for most areas. The most noticeable wind direction errors appear in the area near 12°N and 148°E, where the median filter selects the solution with its direction opposite to the true direction. However, this kind of wind direction errors can be easily corrected by using

Holland's model field for guidance.

It is apparent that the Holland's TC model for Dale is more symmetric than the NSCAT fields. To demonstrate the effects of rain, Fig. 7 illustrates the NSCAT and Holland's TC wind speeds for two cuts through the pixel where the maximum NSCAT wind speeds are found: one parallel to the spacecraft track (along-track) and the other one perpendicular to it (cross-track). At the locations where the SSM/I rain rate were low, there is a qualitative agreement between the NSCAT and Holland's TC winds. However, it appears that the NSCAT wind speeds are significantly lower than the Holland's winds in the high rain areas. This is probably due to the reduction of radar echos from the surfaces by rain, which consequently result in a significant underestimate of NSCAT wind speeds.

To support our hypothesis on the effects of rain a simple radiative transfer model was applied for the analysis of radar cross-sections for hurricane winds: This model assumes a uniform rain rate R_r (mm/h) within a layer of rain with a thickness of H. The rain will attenuate the radar cross-section of the surfaces (σ_0), but will also add backscatter (the second term of the following equation) to the rain-contaminated cross-section measurements (σ_0').

$$\sigma_0' = e^{-2kH/\cos\theta}\sigma_0 + \frac{\cos\theta}{2k}(1 - e^{-2kH/\cos\theta})\frac{9 \times 10^{-11}\pi^5}{\lambda_0^4}Z_r \qquad (7)$$

where the rain reflectivity $Z_r = 200R_r^{1.6}$ and the attenuation coefficient $k = 0.0313R_r^{1.1224}$ [*Ulaby et al.*, 1982]. λ_0 (cm) is the electromagnetic wavelength. Following the SSM/I rain algorithms proposed by Wentz and Spencer [1998], we assume a thickness of 3 km for the rain layer in the tropical regions. Fig. 8 illustrates the model σ_0' as a function of rain rate for the upwind and downwind σ_0s for approximately 33 m·s^{-1} winds at 35°, 45°, and 55° incidence angles. σ_0' decreases initially with increasing rain rate. When the rain rate exceeds 20 mm/hr, the scattering by rain becomes dominant, and the difference between upwind and downwind σ_0's reduces. It appears that the σ_0 could be

reduced by a few dBs. An inspection of Fig. 3 suggests that a few dB reduction of σ_0 will result in a wind speed error by more than 20 m·s^{-1}. Furthermore a reduced upwind and crosswind σ_0 ratio will degrade the direction accuracy of scatterometer winds. This model simulation corroborates the characteristics indicated in Figs. 5 and 6 and signifies the influence of rain on scatterometer winds.

4. Error Analysis

For the situations when the rain rates were low, it seemed that the NSCAT/TC2 winds can reach 30-50 m·s^{-1} in the cyclones (Figs. 5-7 and Table 4). To validate the NSCAT/TC2 winds for tropical cyclones, we find the maximum wind speed in each NSCAT pass of the tropical cyclones (Table 3) and compare it with the JTWC and NHC Dvorak estimates (Fig. 9). Table 4 compares the NSCAT maximum winds with the Dvorak estimates for four passes of Typhoon Dale and one pass of Hurricane Lili. The agreement is remarkable for three of the five cases. It appears that the NSCAT winds can now reach 50 m·s^{-1}, but are frequently lower than the Dvorak estimates. If we assume that the Dvorak technique produces zero-biased estimates, then the NSCAT/TC2 maximum winds underestimate the maximum wind speeds of tropical cyclones. Based on the discussions described earlier on the effects of rain, this indication may not be surprising at all if the locations of maximum winds always have rain.

However, many areas in tropical cyclones can be considerably dry with low rain rates (a few millimeters per hour). This suggests that the NSCAT winds in those areas could be still meaningful. To investigate this possibility, we generate the Holland's TC model winds for every NSCAT pass of tropical cyclones with the Dvorak wind estimates exceeding 32 m·s^{-1}. We evaluate the Holland's model winds at the locations where the NSCAT maximum winds are found. The agreement between NSCAT and Holland's winds is reasonable for 20-50 m·s^{-1} (Fig. 10), although with a considerable scatter. There are several outliers at lower and higher wind speeds, indicated by plus in Fig. 10.

The data point with the Holland wind near 5 $m \cdot s^{-1}$ corresponds to the situation that the center of the NSCAT pixel is located about 14 km to the center of the eye, which is within the eyewall of the model field and hence has a low model wind speed. This could be due to a finite resolution of NSCAT cell (25km by 25 km) with the σ_0 cells encompassing part of the eyewall, where high winds are expected. It is also possible that the interpolation of JTWC/NHC best track could have errors for the actual location of the eye. For the data points with Holland model wind speeds above 50 $m \cdot s^{-1}$, the NSCAT wind speeds are significantly lower. It is likely that the NSCAT/TC2 GMF is erroneous at such an extreme wind velocity. Furthermore, we find that the SSM/I rain rates of these data points are 19.3, 5.1, 10.9, 9.1, and 10.5 mm/h for the five data points in ascending model wind speed order, suggesting that rain could be playing a role in the underestimates of extreme wind speeds.

If these data points are ignored, the agreement is better than the comparison illustrated in Fig. 8 for 20-50 $m \cdot s^{-1}$ winds. A linear-regression of the data marked by open circles with the Holland's winds from 20-50 $m \cdot s^{-1}$ suggests a small bias (< 4 $m \cdot s^{-1}$) in the NSCAT wind estimates. We also plot the data points with the colocated SSM/I rain rates less than 5 mm/h (black filled circles in Fig. 10). The linear regression of the low rain data illustrated by the dashed line shows a slightly increased bias at about 40 $m \cdot s^{-1}$ wind speeds, but the bias is more uniform as a function of wind speed. The small wind speed bias errors suggest that the accuracy of the NSCAT/TC2 GMF is within a few tenths of dB. However, it should be noted that the difference between the NSCAT and Holland's model winds are well within the expected accuracy of the Holland's model wind speed derived from the best track analysis.

5. Discussion and Summary

The accuracy of NSCAT winds for tropical cyclones have been examined with a comparative analysis of satellite data and the best track analysis from JTWC and

NHC for 14 Western Pacific and North Atlantic tropical cyclones from September 1996 through June 1997. The NSCAT data from about 100 satellite passes were processed. It is found that the centers of cyclones frequently fell off the swath of NSCAT, and the data from those passes were excluded for analysis.

Two critical issues pertinent to the accuracy of NSCAT winds for tropical cyclones are explored: One regards the adequacy of the NSCAT GMF and the other one concerns the effects of rain. A comparison of the NSCAT2 GMF with the aircraft scatterometer measurements suggests the corrections of the high wind σ_0 and the ratio of upwind and crosswind σ_0s. We introduced an empirical correction function with its functional form suggested by the influence of various dissipation processes on the amplitude and angular distribution of short-gravity and capillary waves. Subsequent data analysis indicates that the corrections make a positive impact on the accuracy of NSCAT winds for tropical cyclones. However, it is recognized that the NUSCAT/HOWE data are limited in terms of the coverage of incidence angles and there is a lack of aircraft or satellite scatterometer observations with in-situ measurements of surface winds above 40 $\mathrm{m \cdot s^{-1}}$. More extensive aircraft Ku-band scatterometer flights are recommended to fully explore the dependence of σ_0 on surface wind speeds.

The impact of rain is studied by the comparison of NSCAT winds with the SSM/I rain for all the satellite passes for 14 tropical cyclones. However, the time of NSCAT passes was usually different from that of SSM/I passes, and the storms had usually moved during the period of satellite passes. Therefore, extreme care has to be taken when analyzing the colocated NSCAT and SSM/I data. We found a few cases when the storms moved slowly based on the best track analysis. For these cases (only one NSCAT pass of typhoon Dale is illustrated in this article), many of the spiral bands in NSCAT wind images are strongly correlated the SSM/I rain rate distribution. This provides a qualitative indication of the impact of rain. We further examine a radiative transfer scattering model of rain. The model simulations of σ_0 support the indications that rain

tends to reduce the apparent velocity of winds for Ku-band scatterometry. However, we found that the NSCAT winds for typhoon Dale can be as low as 5 $m \cdot s^{-1}$ for areas of heavy rain (above 20 mm/h) near the eye wall. This cannot be explained by the simple radiative transfer scattering model. It is possible that the rain might have significantly damped the short ocean waves, which contribute to the Ku-band radar scattering. More extensive analysis of the NSCAT σ_0 and SSM/I rain data, such as the study by [*Smith and Wentz*, 1998], is suggested to better quantify the influence of rain on Ku-band ocean radar scattering.

Our study has shown that the modified NSCAT GMF (NSCAT/TC2) can produce wind speeds in the range of 30-50 $m \cdot s^{-1}$. A comparison with the Holland's TC model fields suggests that it is possible to observe 30-50 $m \cdot s^{-1}$ winds with a spaceborne Ku-band scatterometers, provided that the rain rates are low (less than a few mm/h). For low rain areas, the bias error derived from the regression analysis are less than 3-4 $m \cdot s^{-1}$ with respect to Holland's model winds.

Acknowledgments. The research carried out in this paper is performed by the Jet Propulsion Laboratory under a contract with the National Aeronautics and Space Administration. The research is supported in part by the NASA Scatterometer (NSCAT) Project. We are grateful to the Remote Sensing Systems for making the daily SSM/I products available for this investigation.

References

Bender, M. A., R. J. Ross, R. E. Tuleya, and Y. Kurihara, Improvements in Tropical cyclone Track and Intensity Forecasts Using the GFDL Initialization System, *Monthly Weather Review*, Vol. 121, 2046–2061, 1993.

Carswell, J., S. C. Carson, R. E. McIntosh, F. K. Li, G. Neumann, D. J. Mclaughlin, J. C. Wilkerson, P. G. Black, and S. V. Nghiem, Airborne Scatterometers: Investigating Ocean Backscatter Under Low- and High-Wind Conditions, *Proc. IEEE.* Vol. 82, No. 12, 1835–1860, 1994.

Dickinson, S. and R. A. Brown, A Study of Near-Surface Winds in Marine Cyclones Using Multiple Satellite Sensors, *J. Appl. Meteorology*, Vol. 35, 769-781, June 1996.

Dvorak, V. F., Tropical Cyclone Intensity Analysis and Forecasting from Satellite Imagery, *Monthly Weather Review*, Vol. 103, 420–430, 1975.

Holland, G., An Analytic Model of the Wind and Pressure Profiles in Hurricanes, *Monthly Weather Review*, Vol. 108, 1212–1218, 1980.

Hsu, C. and W. T. Liu, Wind and Pressure Fields Near Tropical Cyclone Oliver Derived From Scatterometer Observations, *J. Geophys. Res.*, 101(D12), 17021-17027, July 1996.

Hsu, C. S., W. T. Liu, and M. G. Wurtele, Impact of Scatterometer Winds on Hydrologic Forcing and Convective Heating Through Surface Divergence, *Monthly Weather Review*, Vol. 125(7), 1556-1576 (1997 Jul).

Liu, Y., and X.-H. Yan, The Wind-Induced Wave Growth Rate and the Spectrum of the Gravity-Capillary Waves, *J. of Phys. Oceanography*, Vol. 25, 3196–3218, 1995.

Naderi, F. M., M. H. Freilich, and D. G. Long, Spaceborne Radar Measurement of Wind Velocity Over the Ocean — An Overview of the NSCAT Scatterometer System, *Proc. of The IEEE*, Vol. 79, No. 6, 850–866, 1991.

Quilfen, Y., B. Chapron, T. Elfouhaily, K. Katsaros and J. Tournadre, Observation of Tropical Cyclones by High-Resolution Scatterometry, *J. Geophys. Res.*, 103(C4), 7767-7786, April 1998.

Smith, D. K., and F. Wentz, Correction of Rain Affected NSCAT Winds, *Proc. of 1998 Fall*

AGU Meeting, San Francisco, 1998.

Stoffelen, A. and D. Anderson, "Scatterometer data interpretation: Estimation and validation of the transfer function CMOD4," *J. Geophys. Res.*, Vol. 102, No. C3, pp. 5767-5780, March 15, 1997.

Ulaby, F. T., R. K. Moore, and A. K. Fung, Microwave Remote Sensing: Fundamentals and Radiometry, Section 5-12, Vol. 1, Artech House, Norwood, Massachusettts, 1982.

Wentz, F. J., M. H. Freilich, and D. K. Smith, NSCAT-2 Geophysical Model Function, *Proc. of 1998 Fall AGU Meeting*, San Francisco, 1998.

Wentz, F. J., and R. W. Spencer, SSM/I Rain Retrievals within a Unified All-Weather Ocean Algorithm, *J. Atmospheric Sci.*, Vol. 55, No. 6, 1613–1627, 1998.

Young, I. R., An Estimate of the Geosat Altimeter Wind Speed Algorithm at High Wind Speeds, *J. Geophys. Res.*, 98(C11), 20,275-20,285, November 1993.

Yueh, S. H., R. West, F. Li, W.-Y. Tsai and R. Lay, Dual-Polarized Ku-band Backscatter Signatures of Hurricane Ocean Winds, accepted for publication in *IEEE Geosci. and Remote Sens.*, 1999.

S. H. Yueh, W.-Y. Tsai, C. S. Hsu, H. Hua and W. T. Liu, Jet Propulsion Laboratory, California Institute of Technology, 4800 Oak Grove Drive, Pasadena, CA 91109. (e-mail: simon.yueh@sjpl.nasa.gov; wtsai@pop.jpl.nasa.gov; csh@seastore.jpl.nasa.gov; hxh@pacific.jpl.nasa.gov; liu@pacific.jpl.nasa.gov)

Received _____

Table 1. Polynomial expansion coefficients for the ratios of upwind and crosswind σ_0s for vertical polarization

Parameter	a_0	a_1	a_2	a_3
c	-0.742	0.1971	-5.0335×10^{-4}	-7.6889×10^{-6}
a	24.6143	-1.0272	0.01818	-1.06×10^{-4}
b	17.827	0.60859	-0.024436	2.0684×10^{-4}
α	3	0	0	0
β	1.5876	0.064281	-8.3757×10^{-4}	2.6808×10^{-6}
γ_1	1.5365	-0.05872	1.2747×10^{-3}	-8.53827×10^{-6}
γ_2	0.8	0	0	0

Table 2. Polynomial expansion coefficients for the ratios of upwind and crosswind σ_0s for horizontal polarization

Parameter	a_0	a_1	a_2	a_3
c	-3.133	0.4451	-7.7443×10^{-3}	4.3689×10^{-5}
a	16.002	-0.1502	-7.6829×10^{-3}	1.2419×10^{-4}
b	12.032	1.04744	-3.1304×10^{-2}	2.3184×10^{-4}
α	3	0	0	0
β	2.5688	0.026447	-2.1273×10^{-3}	2.6932×10^{-5}
γ_1	1.6600	-0.06740	1.4050×10^{-3}	-9.2657×10^{-6}
γ_2	1.0099	-0.01553	2.0833×10^{-4}	-4.7536×10^{-7}

Table 3. Summary of the Western Pacific and North Atlantic cyclones analyzed. The fourth column indicates the number of NSCAT passes with the Dvorak estimates of maximum wind speed exceeding 64 knots. The number in the parenthesis indicates the number of passes when the cyclone center was in the swath.

Name	Date	Location	Number of NSCAT Passes
Tom	Sep 1996	Pacific	4(2)
Willie	Sep 1996	Pacific	5(1)
Violet	Sep 1996	Pacific	10(6)
Yates	Sep 1996	Pacific	8(5)
Zane	Sep 1996	Pacific	9(5)
Beth	Oct 1996	Pacific	6(5)
Dale	Nov 1996	Pacific	12(4)
Fern	Dec 1996	Pacific	3(3)
Marie	May 1997	Pacific	1(1)
Nester	June 1997	Pacific	3(3)
Opal	June 1997	Pacific	3(3)
Peter	June 1997	Pacific	3(2)
Isidore	Sep 1996	Atlantic	2(2)
Lili	Oct 1996	Atlantic	5(1)

Table 4. NSCAT/TC2 and JTWC/Dvorak estimates of the maximum wind speed for one pass of Hurricane Lili and four NSCAT passes of typhoon Dale.

Name	Date	UTC Time	NSCAT/TC2	JTWC/NHC
Lili	Oct 19, 1996	3:54	43	44
Dale	Nov 7, 1996	1:04	36.8	38
Dale	Nov 8, 1996	13:20	45.1	46
Dale	Nov 10, 1996	14:08	48.1	70
Dale	Nov 11, 1996	2:33	38.5	65

Figure 1. NUSCAT σ_0 and radiometer data acquired from the HOWE 1997 versus the relative azimuth angle between the wind and radar look directions. σ_{vv} denotes the normalized radar cross sections for vertically polarized transmit and vertically polarized receive, σ_{hh} for horizontally polarized transmit and horizontally polarized receive, and σ_{hv} for vertically polarized transmit and horizontally polarized receive. The bottom panel plots the vertically and horizontally polarized brightness temperatures (T_v and T_h). The wind measured by the GPS dropsonde was 35 m·s^{-1}. The incidence angle is 45° for NUSCAT and 55° for the radiometer.

Figure 2. NUSCAT σ_0 data acquired from the HOWE 1997 versus the relative azimuth angle between the wind and radar look directions. The wind measured by the GPS dropsonde was 30 m·s^{-1}. The incidence angle is 55° for NUSCAT and 65° for the radiometer.

Figure 3. Upwind and crosswind σ_0s from NSCAT2 and NSCAT/TC2 geophysical model functions and the NUSCAT/HOWE aircraft scatterometer measurements at 35, 46, and 54 degree incidence angles. The upper panels are for vertical polarization and the lower panels for horizontal polarization.

Figure 4. r_{uc} and r_{ud} in dB from NSCAT2 and NSCAT/TC2 geophysical model function and NUSCAT aircraft scatterometer measurements for vertical polarization

Figure 5. NSCAT Images of Typhoon Dale in November 1996. Black filled circles represent the center of cyclones.

Figure 6. Comparison of NSCAT, SSM/I, and Holland Model winds for Typhoon Dale, November 7, 1996. The SSM/I wind speed, cloud liquid water and water vapor are also included for comparison. Areas of heavy rains are associated with high cloud liquid water content.

Figure 7. Along- and cross-track cuts of NSCAT/TC2 winds for typhoon Dale and SSM/I rain rate. The cuts are through the location where the maximum NSCAT wind is found. For convenience, the along-track cut is plotted as a function of latitude, and the cross-track cut as a function of longitude.

Figure 8. Theoretical Ku-band radar cross-sections of ocean surfaces in the presence of a uniform rain layer at 35°, 45° 55° incidence angle. The rain-free σ_0s approximately correspond to a wind speed of 33 m·s^{-1} at upwind and crosswind directions indicated in Fig. 3.

Figure 9. NSCAT maximum wind speed versus Dvorak Wind. The Dvorak wind was linearly interpolated from the JTWC/HC best track analysis at the time of NSCAT passes.

Figure 10. NSCAT maximum wind speeds versus Holland model winds. The Holland's TC model parameters were selected based on the JTWC/NHC best track analysis. Black-filled and open circles represent the data with the model wind speed within 20-50 m·s^{-1}. The data with SSM/I rain rates less than 5 mm/h are indicated by black filled circles. The solid curve (dashed line) is the linear regression of the data indicated by open circles (black filled circles).

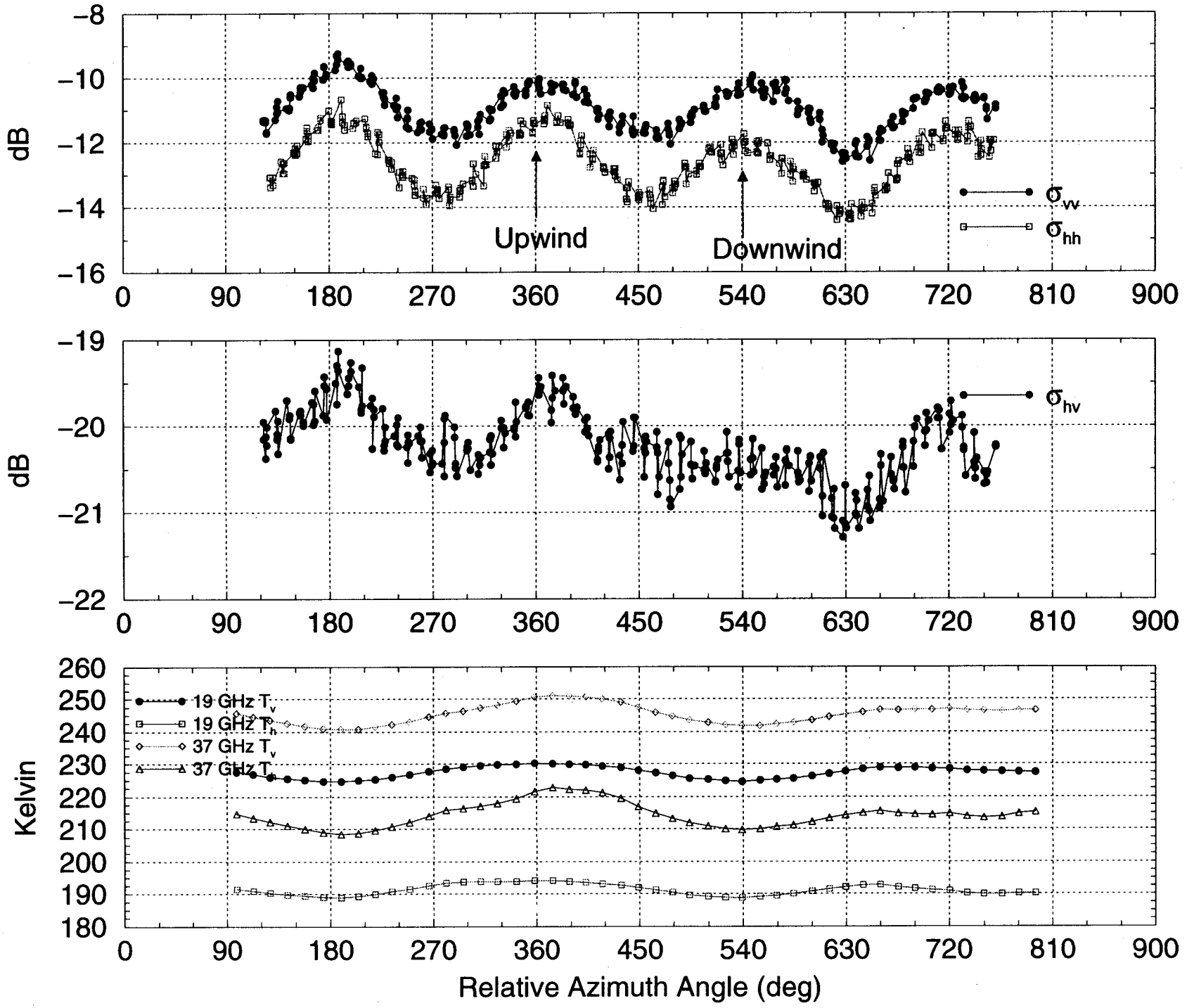
dB
−8
−10
−12
−14
−16
Upwind
Downwind
σ_{vv}
σ_{hh}
dB
−19
−20
−21
−22
σ_{hv}
Kelvin
260
250
240
230
220
210
200
190
180
19 GHz T_v
19 GHz T_h
37 GHz T_v
37 GHz T_h
0
90
180
270
360
450
540
630
720
810
900
Relative Azimuth Angle (deg)

Fig. 1

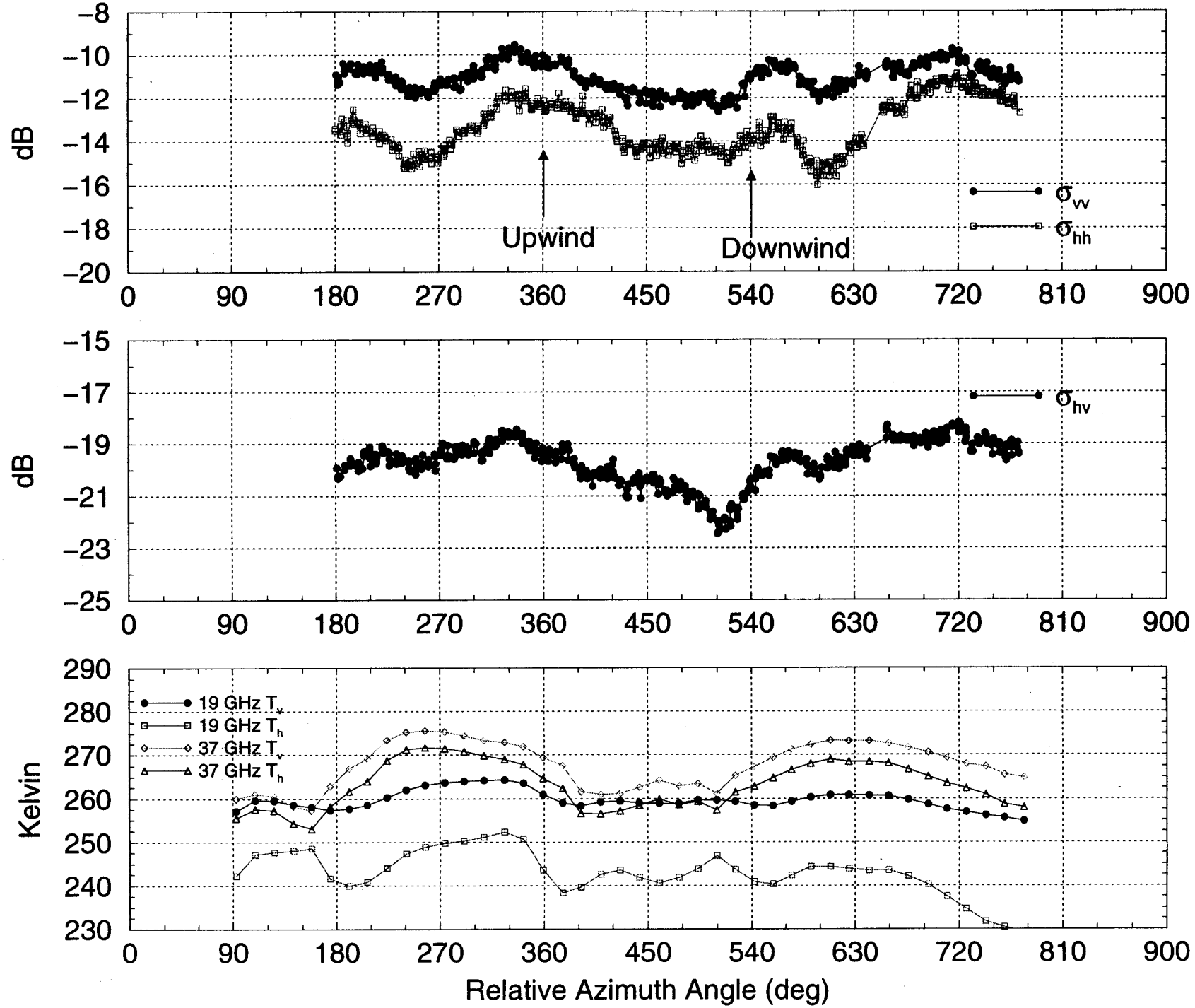
dB
−8
−10
−12
−14
−16
−18
−20
Upwind
Downwind
σ_{vv}
σ_{hh}
0
90
180
270
360
450
540
630
720
810
900
dB
−15
−17
−19
−21
−23
−25
σ_{hv}
Kelvin
290
280
270
260
250
240
230
19 GHz T_v
19 GHz T_h
37 GHz T_v
37 GHz T_h
Relative Azimuth Angle (deg)

Fig. 2

COMPARISON OF NSCAT2/TC–2 MODEL FUNCTIONS WITH NUSCAT OBSERVATIONS OF HURRICANE ERIKA

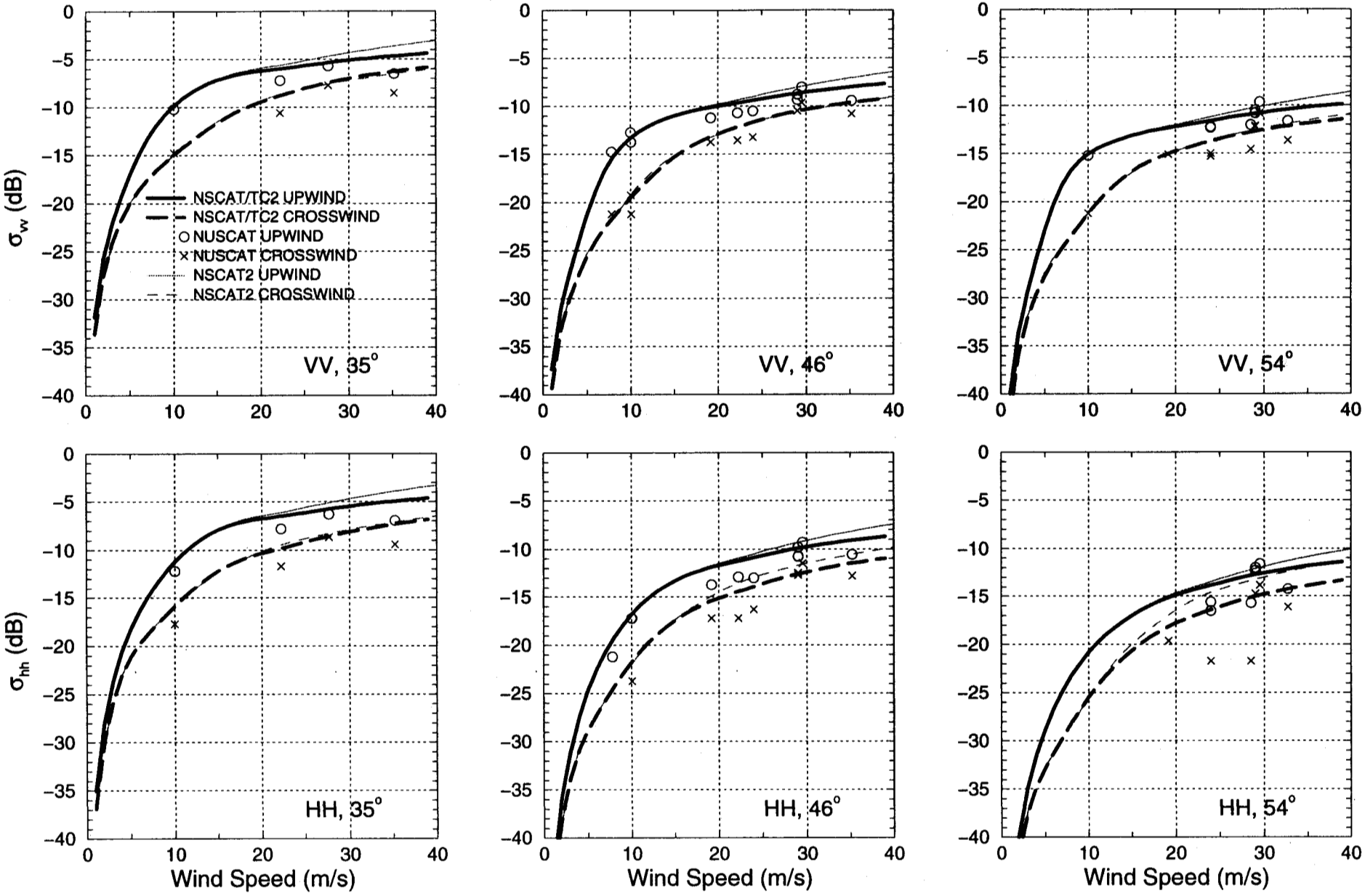

Fig.3

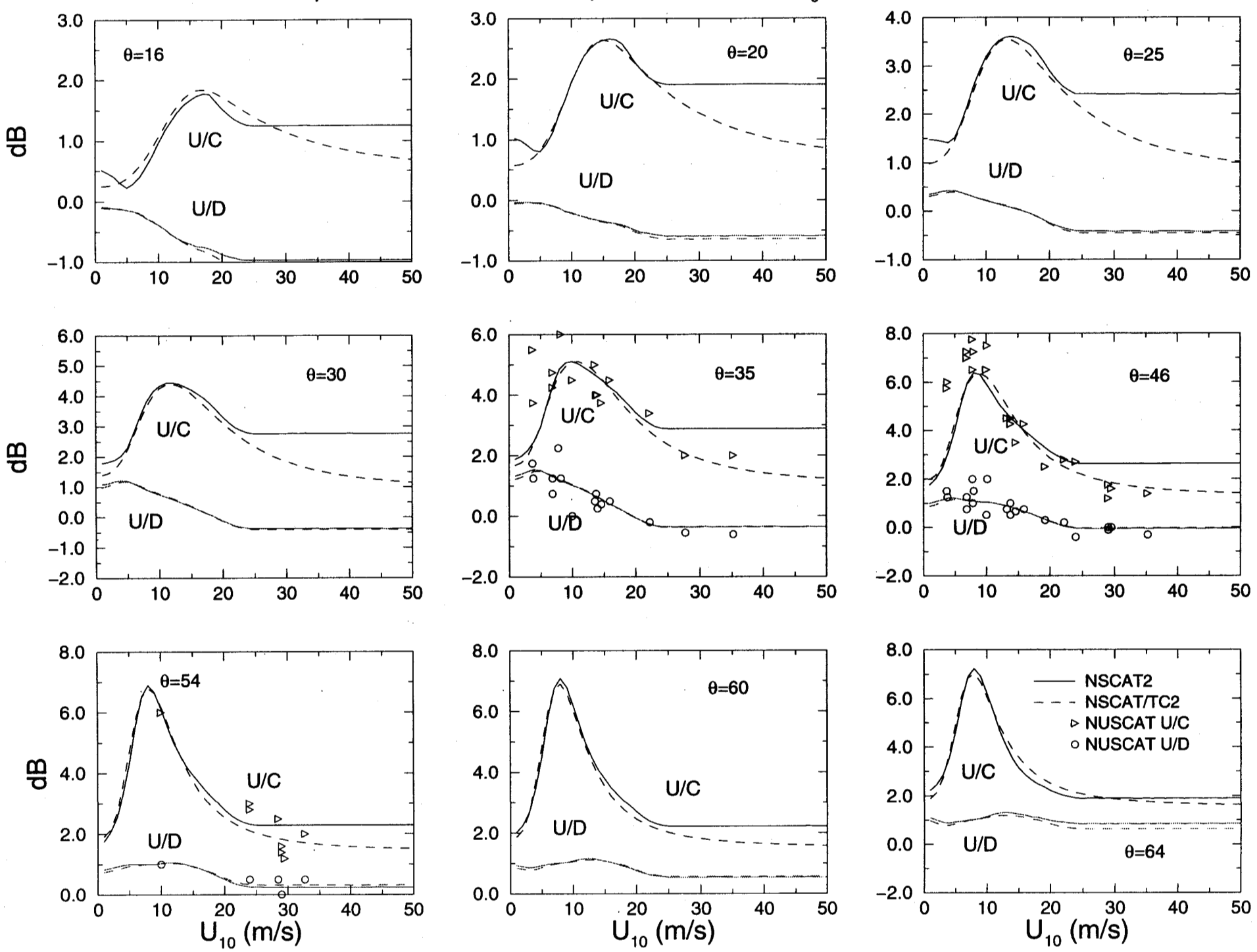
Upwind/Crosswind and Upwind/Downwind σ_0 RATIOS (V–POL)
θ=16
θ=20
θ=25
θ=30
θ=35
θ=46
θ=54
θ=60
θ=64
U/C
U/D
dB
U_{10} (m/s)
NSCAT2
NSCAT/TC2
NUSCAT U/C
NUSCAT U/D

Fig 4

NSCAT TC Winds

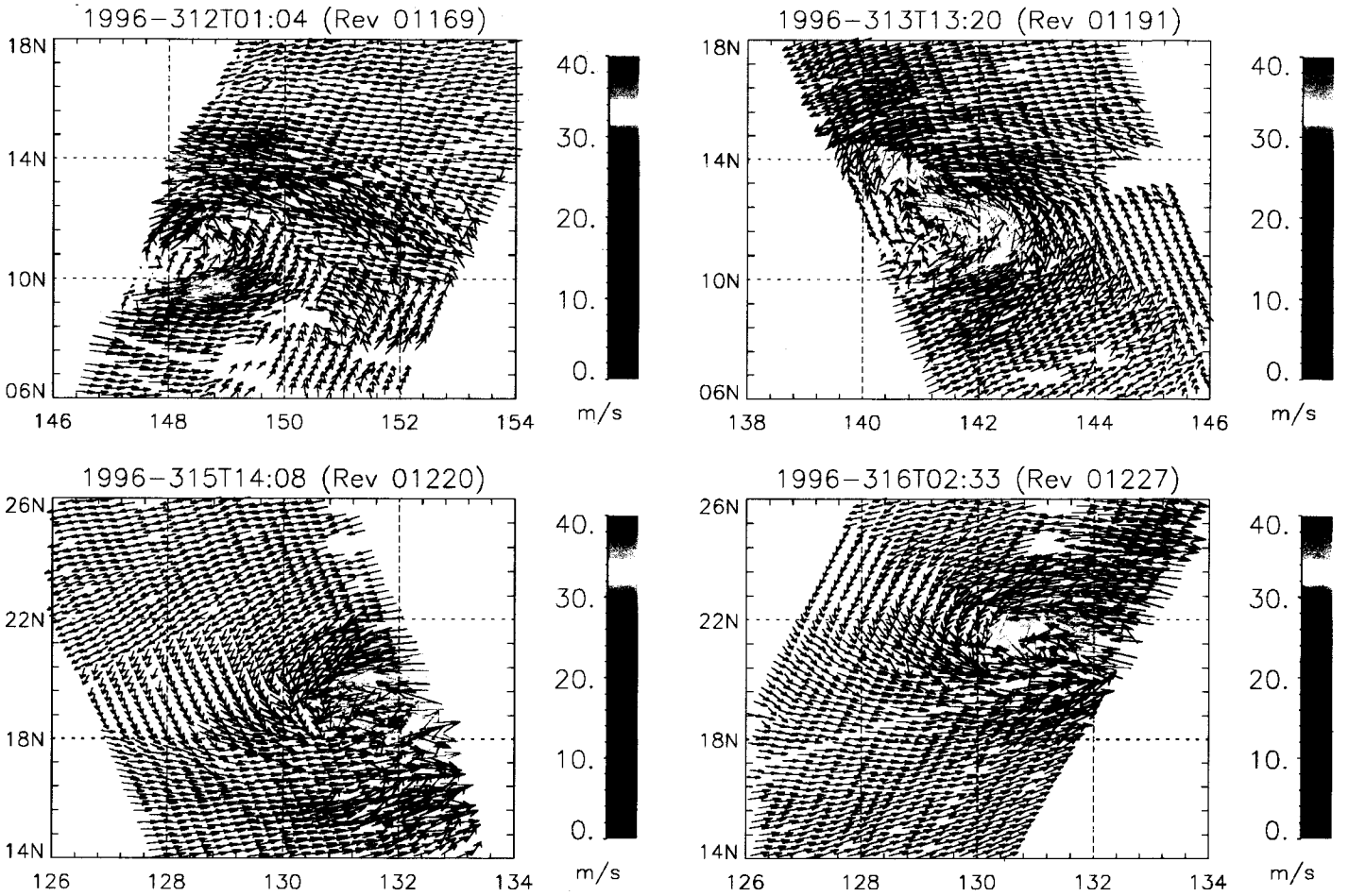

NSCAT Wind, SSM/I Products and TC Model Comparison

SSM/I Wind Speed (961107)

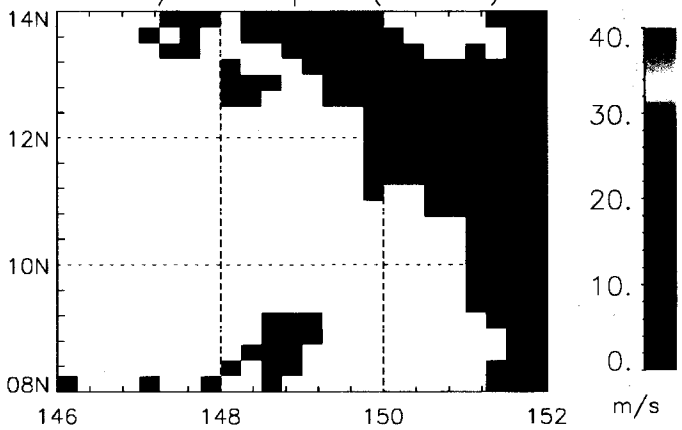

SSM/I Liquid Water (961107)

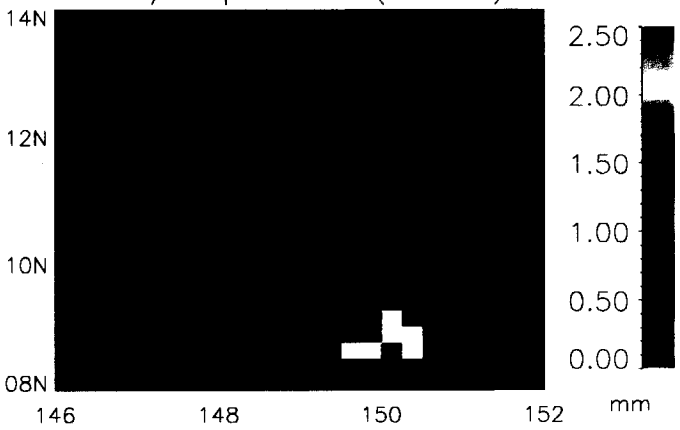

SSM/I Water Vapor (961107)

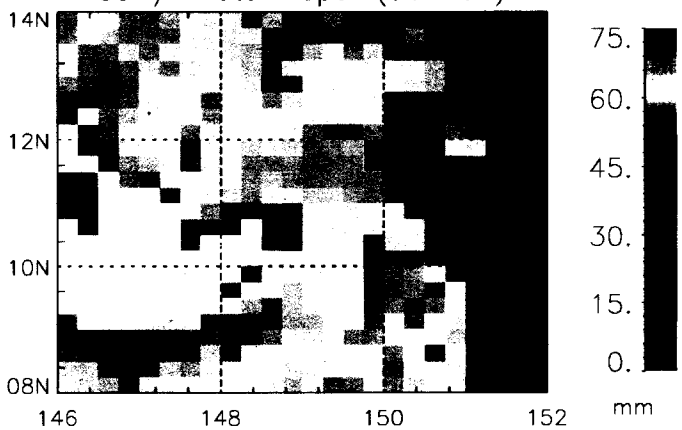

SSM/I Rain (961107)

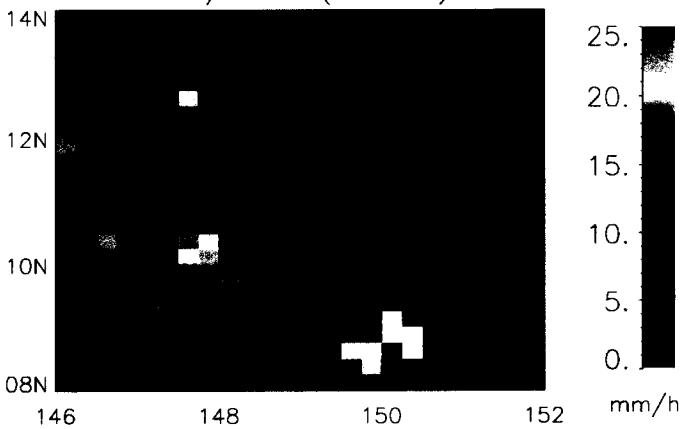

NSCAT Winds – Dale (Rev 01169)

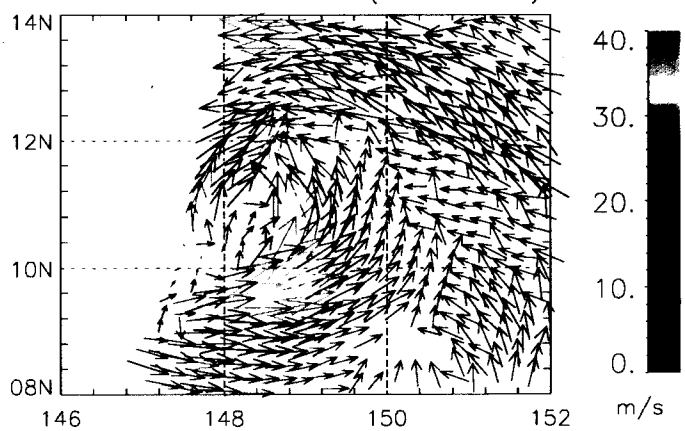

Holland TC Model

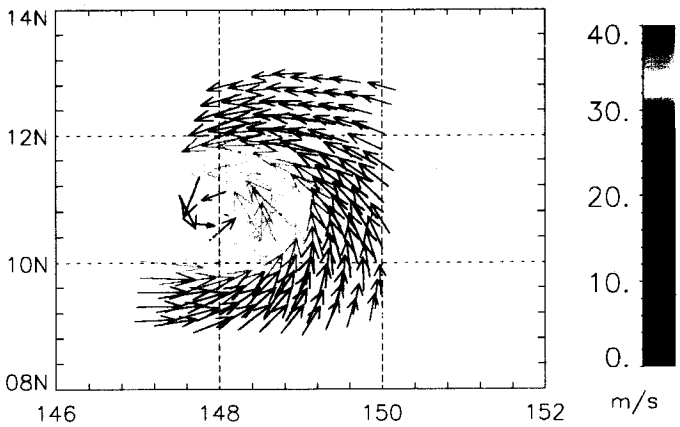

NSCAT Max Speed 36.8 m/s

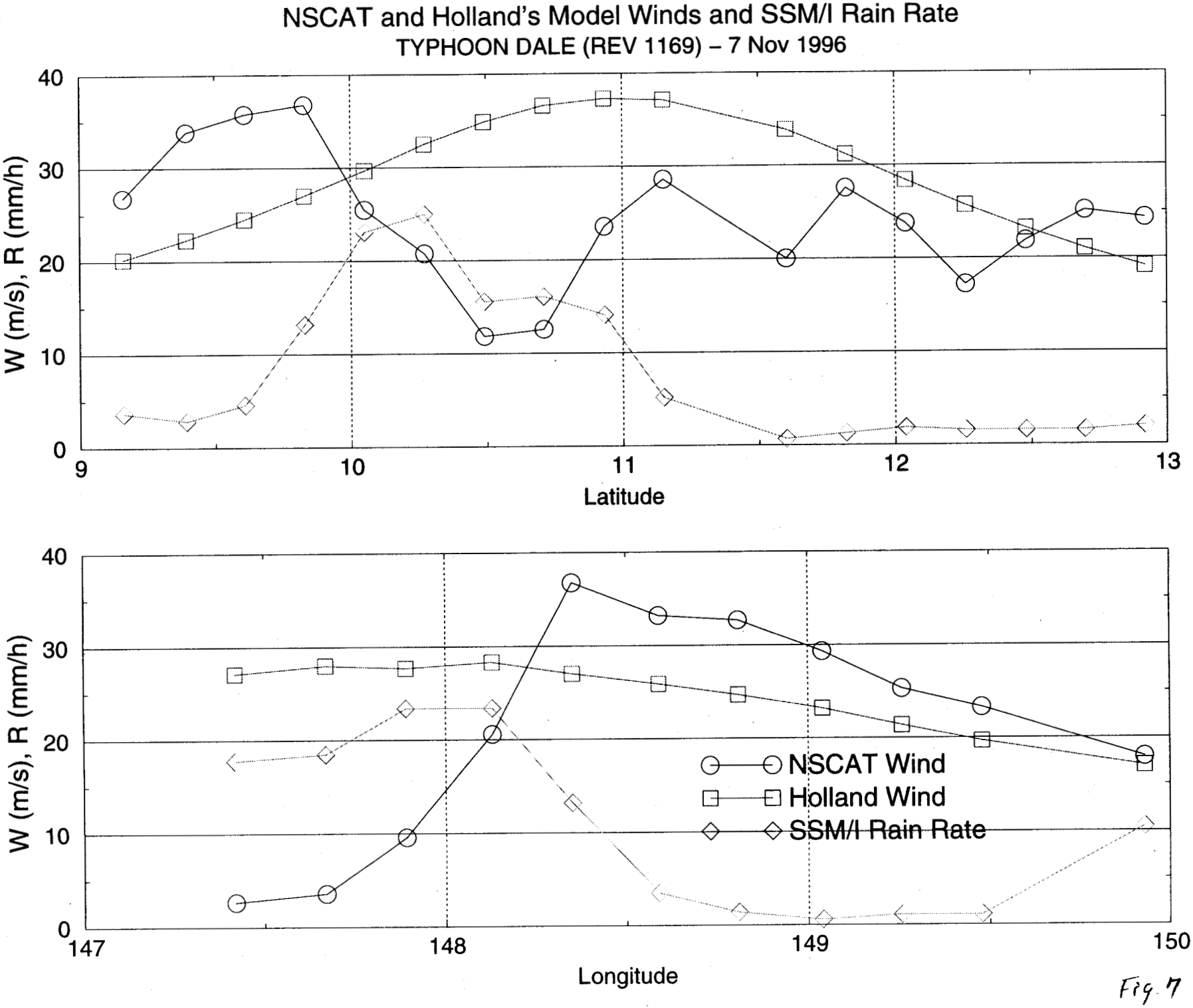
NSCAT and Holland's Model Winds and SSM/I Rain Rate
TYPHOON DALE (REV 1169) – 7 Nov 1996
W (m/s), R (mm/h)
Latitude
Longitude
NSCAT Wind
Holland Wind
SSM/I Rain Rate

Fig. 7

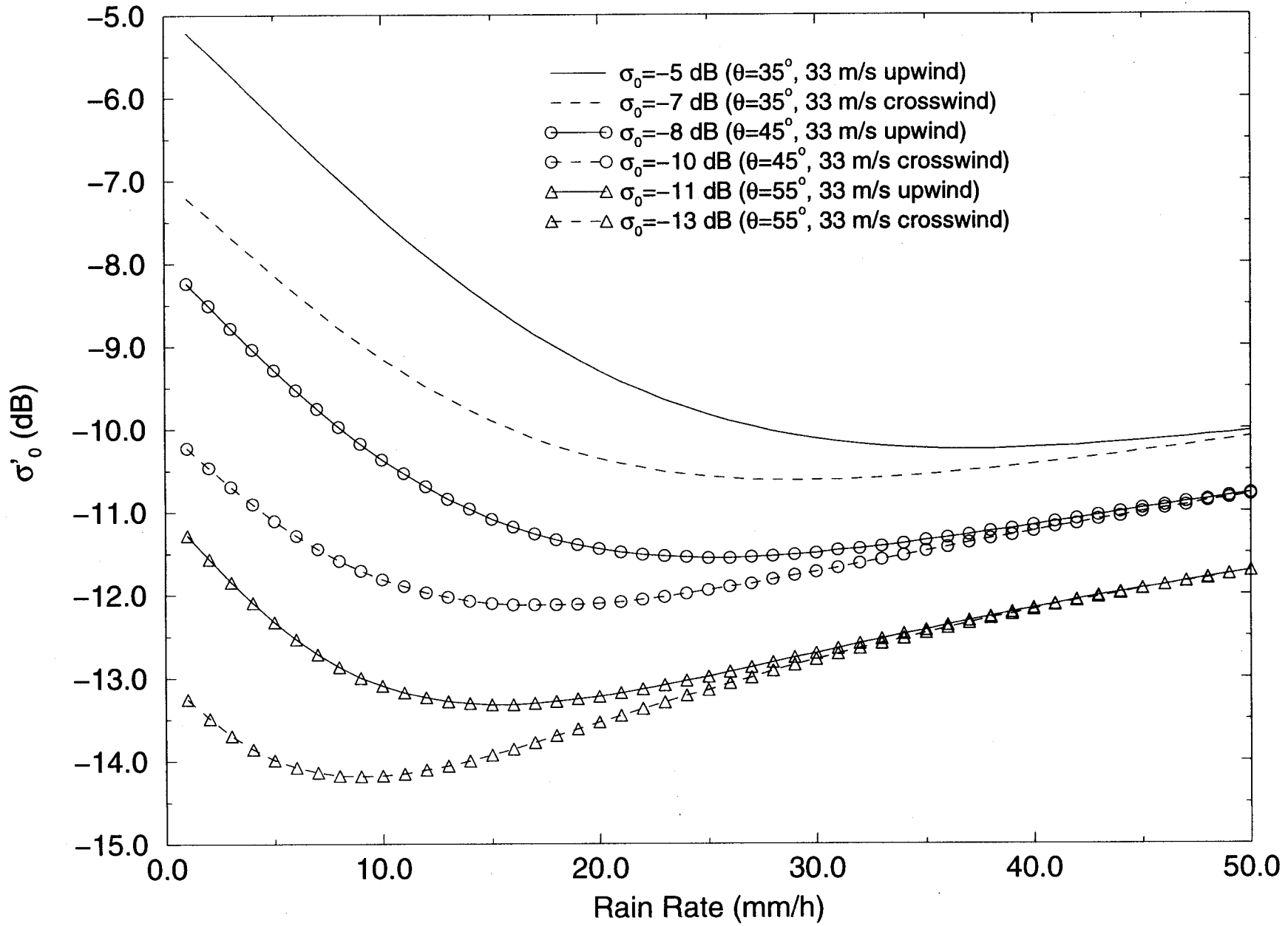
σ0=−5 dB (θ=35°, 33 m/s upwind)
σ0=−7 dB (θ=35°, 33 m/s crosswind)
σ0=−8 dB (θ=45°, 33 m/s upwind)
σ0=−10 dB (θ=45°, 33 m/s crosswind)
σ0=−11 dB (θ=55°, 33 m/s upwind)
σ0=−13 dB (θ=55°, 33 m/s crosswind)
σ'0 (dB)
−5.0
−6.0
−7.0
−8.0
−9.0
−10.0
−11.0
−12.0
−13.0
−14.0
−15.0
0.0
10.0
20.0
30.0
40.0
50.0
Rain Rate (mm/h)

Fig. 8

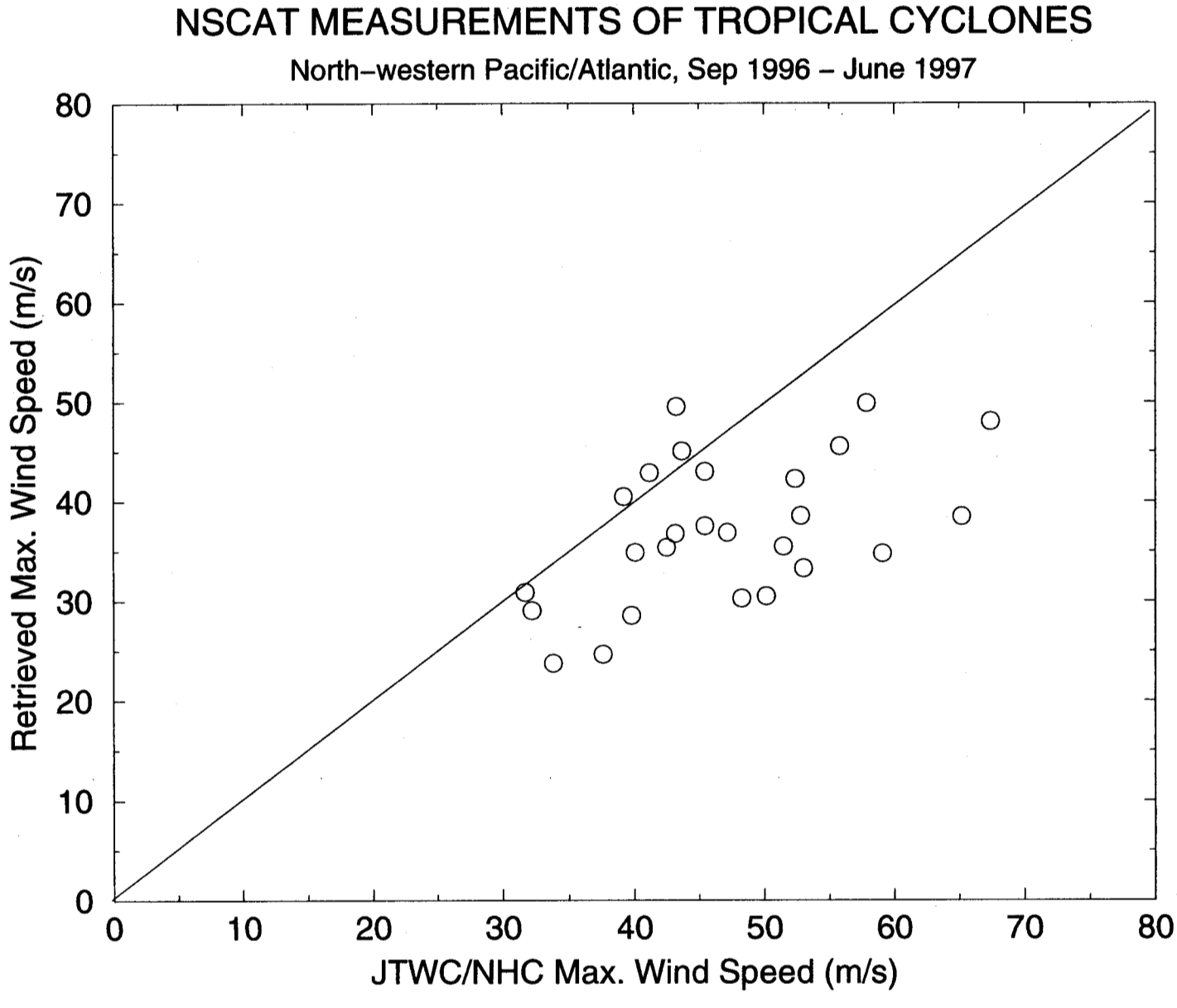
NSCAT MEASUREMENTS OF TROPICAL CYCLONES
North–western Pacific/Atlantic, Sep 1996 – June 1997
Retrieved Max. Wind Speed (m/s)
JTWC/NHC Max. Wind Speed (m/s)
0
10
20
30
40
50
60
70
80

Fig. 9

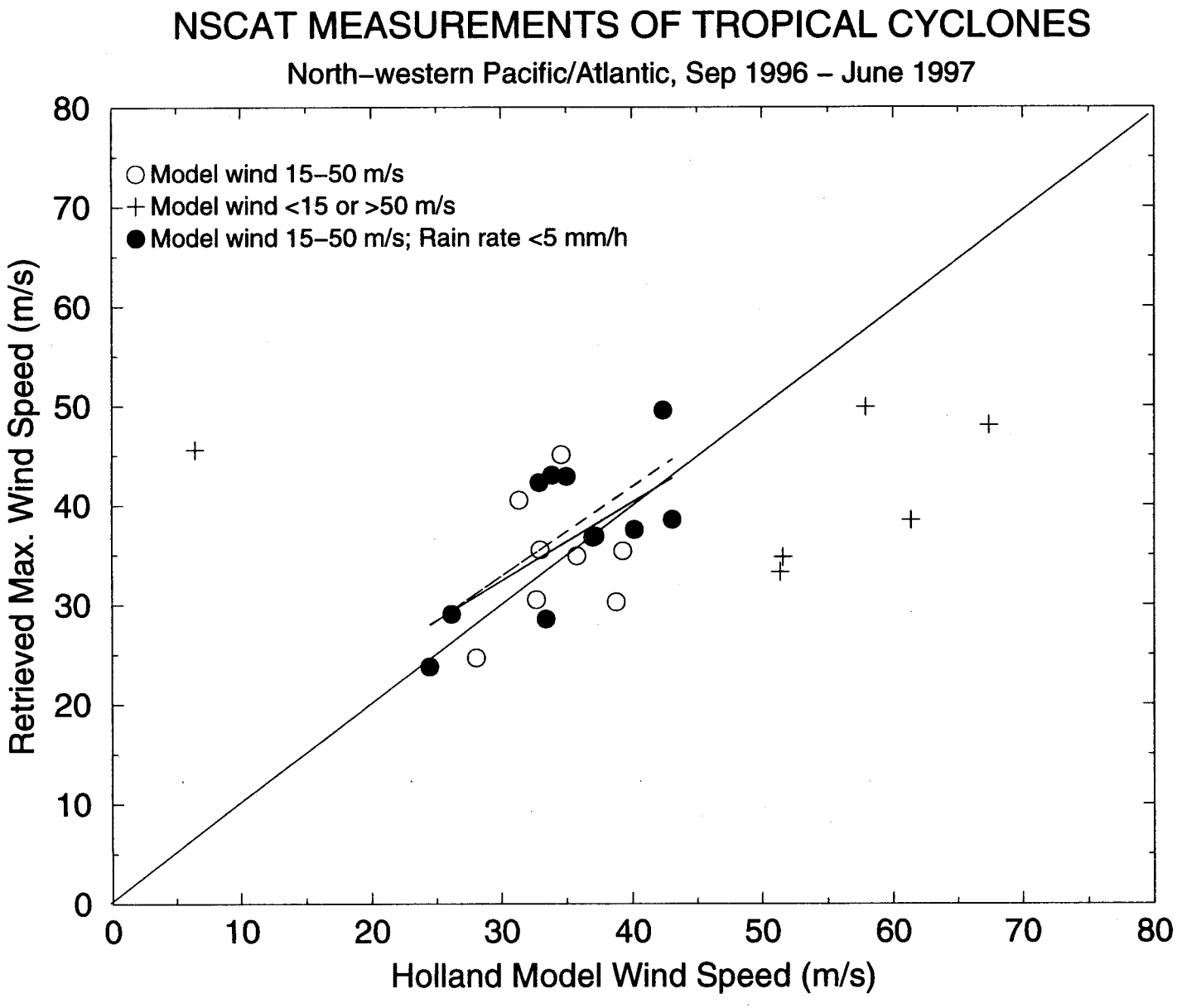
NSCAT MEASUREMENTS OF TROPICAL CYCLONES
North–western Pacific/Atlantic, Sep 1996 – June 1997
Model wind 15–50 m/s
Model wind <15 or >50 m/s
Model wind 15–50 m/s; Rain rate <5 mm/h
Retrieved Max. Wind Speed (m/s)
Holland Model Wind Speed (m/s)
0
10
20
30
40
50
60
70
80

Fig. 10